Mon. Not. R. Astron. Soc. **357,** 242–250 (2005) doi:10.1111/j.1365-2966.2005.08643.x

Buoyant radio lobes in a viscous intracluster medium

Christopher S. Reynolds,[1★] Barry McKernan,[1] Andrew C. Fabian,[2] James M. Stone[3] and John C. Vernaleo[1]

[1]*Department of Astronomy, University of Maryland, College Park, MD 20742, USA*
[2]*Institute of Astronomy, Madingley Road, Cambridge CB3 OHA*
[3]*Department of Astrophysical Sciences, Peyton Hall, Princeton, NJ08544, USA*

Accepted 2004 November 15. Received 2004 November 9; in original form 2004 February 20

ABSTRACT

Ideal hydrodynamic models of the intracluster medium (ICM) in the core regions of galaxy clusters fail to explain both the observed temperature structure of this gas, and the observed morphology of radio-galaxy/ICM interactions. It has recently been suggested that, even in the presence of reasonable magnetic fields, thermal conduction in the ICM may be crucial for reproducing the temperature floor seen in many systems. If this is indeed correct, it raises the possibility that other transport processes may be important. With this motivation, we present a numerical investigation of the buoyant evolution of AGN-blown cavities in ICM that has a non-negligible shear viscosity. We use the ZEUS-MP code to follow the three-dimensional evolution of an initially static, hot bubble in a β-model ICM atmosphere with varying degrees of shear viscosity. With no explicit viscosity, it is found that the combined action of Rayleigh–Taylor and Kelvin–Helmholtz instabilities rapidly shred the ICM cavity and one does not reproduce the intact and detached 'ghost cavities' observed in systems such as Perseus-A. On the other hand, even a modest level of shear viscosity (corresponding to approximately 25 per cent of the Spitzer value) can be important in quenching the fluid instabilities and maintaining the integrity of the bubble. In particular, we show that the morphology of the north-west ghost cavity found in Perseus-A can be reproduced, as can the flow pattern inferred from the morphology of Hα filaments. Finally, we discuss the possible relevance of ICM viscosity to the fact that many of the active ICM cavities (i.e. those currently associated with active radio lobes) are not bounded by strong shocks, the so-called 'shock problem'.

Key words: hydrodynamics – cooling flows – galaxies: jets – X-rays: galaxies: clusters.

1 INTRODUCTION AND OBSERVATIONAL BACKGROUND

Recent years have seen a growing realization that the cores of rich galaxy clusters are complex and dynamic environments. In particular, it is becoming clear that the radio-loud active galactic nuclei (AGN) often hosted by the cD galaxies in rich clusters can have a major influence on the hydrodynamics and thermodynamics of the core regions of the intracluster medium (ICM). As we discuss below, the rich data sets coming from the *Chandra* X-ray Observatory and *XMM–Newton* now demand theoretical models that go beyond the simple picture of jet-blown 'bubbles' rising in a static ICM described by ideal hydrodynamics. Bulk ICM motions (including turbulence), magnetohydrodynamics (MHD), thermal conductivity, and viscosity may all be relevant to data that are currently being taken.

Even before the launches of *Chandra* and *XMM–Newton*, *Einstein* and *ROSAT* studies revealed prominent radio-galaxy/cluster interactions in three clusters: Perseus-A (Böhringer et al. 1993; Heinz, Reynolds & Begelman 1998), Virgo-A (Feigelson et al. 1987; Böringer et al. 1995) and Cygnus-A (Carilli, Perley & Harris 1994; Harris, Carilli & Perley 1994). *ROSAT* showed Perseus-A and Cygnus-A to possess intracluster medium (ICM) cavities coincident with the prominent radio lobes in these two sources, suggesting supersonic inflation of a bubble in the ICM by the jetted AGN (Clarke, Harris & Carilli 1997). Virgo-A, on the other hand, showed a cooler (and soft X-ray brighter) region of ICM associated with the outer eastern 'ear' seen in low-frequency radio maps of Virgo-A (Owen, Eilek & Kassim 2000). It was first suggested by Böringer et al. (1995) that this phenomenon might be caused by lower entropy gas from the cluster centre being dragged upwards in the ICM atmosphere by a buoyantly rising radio lobe.

★E-mail: chris@astro.umd.edu

More recent observations by *Chandra* and *XMM–Newton* show that radio-galaxy induced ICM substructure is surprisingly ubiquitous and complex. The basic results described above, i.e. the existence of ICM cavities associated with active radio lobes and the presence of cool material that appears to lie in the wake of old, buoyantly rising radio lobes, have been confirmed in numerous systems (e.g. Hydra-A, McNamara et al. 2000; Abell 2052, Blanton et al. 2001; Virgo-A, Young, Wilson & Mundell 2002; Perseus-A, Fabian et al. 2000, 2003a). However, these new data have raised several mysteries and are increasingly at odds with simple models for radio-galaxy/ICM interactions. First, in any ideal hydrodynamic model, the cavities must be inflated supersonically or else they would be destroyed by Rayleigh–Taylor (RT) instabilities faster than they are inflated. Curiously, the strong and hot ICM shocks that one expects to find around the active cavities are notably absent; instead, many ICM cavities are surrounded by ICM shells that are *cooler* than the ambient ICM. We shall refer to this as the ‘shock problem’. Secondly, ICM cavities that are not associated with any obvious radio lobe (‘ghost cavities’) have been discovered. Examples are found in the Perseus cluster (Fabian et al. 2003a), Abell 2597 (McNamara et al. 2001), and Abell 4059 (Heinz et al. 2002; Choi et al. 2004). In some cases, ghost cavities are coincident with regions of low-frequency (74 MHz) radio emission supporting the hypothesis that they correspond to old radio lobes from previous and now extinct AGN outbursts (Fabian et al. 2002a). Interestingly, as we will explicitly demonstrate in this paper, ideal hydrodynamic models fail to reproduce the observed morphology of at least some ghost cavities. Finally, most clusters have been found to possess a ‘temperature floor’ in the sense that the radiative cooling of the ICM appears not to proceed below temperatures of $kT \sim 1$–2 keV (Peterson et al. 2001; Tamura et al. 2001). Again, no clear explanation for this fact is provided by an ideal hydrodynamic model. Brüggen & Kaiser (2002) suggest that stirring of the ICM core by a central radio galaxy may be responsible for the temperature floor; however, such a scenario only postpones rather than prevents radiative cooling, and is hard to reconcile with the strong metallicity gradients observed in the cores of some clusters (David et al. 2001; Matsushita et al. 2002; Sanders & Fabian 2002). This has led several authors (Narayan & Medvedev 2001; Fabian, Voigt & Morris 2002b; Voigt et al. 2002; Kim & Narayan 2003) to resurrect the notion that thermal conduction may be important in determining the thermodynamics of ICM cores.

Faced with the multiple failures of simple hydrodynamic models for cluster cores, we must carefully examine the other physical processes that might be relevant. Both the dynamical and thermodynamical effects of magnetic fields are largely unexplored and are the subject of on-going large-scale simulations. However, the qualitative success of models including thermal conduction in solving the temperature-floor problem begs a study of other transport processes and, in particular, the effects of shear viscosity on the dynamics of a radio-galaxy/ICM interaction.

Perseus-A and the core of the Perseus cluster continues to be one of the best-studied examples of a rich cluster core and a complex radio-galaxy/cluster interaction. The most detailed X-ray investigation to date, based on a deep (200 ks) observation by *Chandra*/ACIS-S, has been presented by Fabian et al. (2003a). These authors report the discovery of wave-like disturbances in the ICM on spatial scales of ~50 kpc, approximately twice the spatial scales of the most obvious ghost cavity to the north-west of Perseus-A. They discuss a scenario in which viscous dissipation of these disturbances may act as a significant heat source for the ICM core. It is shown that, provided viscosity operates reasonably close to its ideal unmagnetized value, it is possible for viscous dissipation of radio-galaxy induced disturbances to balance radiative cooling of the ICM. This suggestion has been supported by recent simulation work by Ruszkowski, Brüggen & Begelman (2004). Circumstantial evidence for the presence of significant ICM viscosity is also provided by an examination of the morphology of Hα filaments. Several of the filaments appear to trace well-defined arcs in the region below the ghost cavity (Fig. 1; also see Fabian et al. 2003b). This argues against the presence of strong turbulence in the ICM core, possibly resulting from the action of viscosity. If we make the stronger presumption that the Hα filaments follow streamlines in the ICM, the morphology of the filaments suggests the existence of a vortex ring within the ICM just below the north-west ghost cavity.

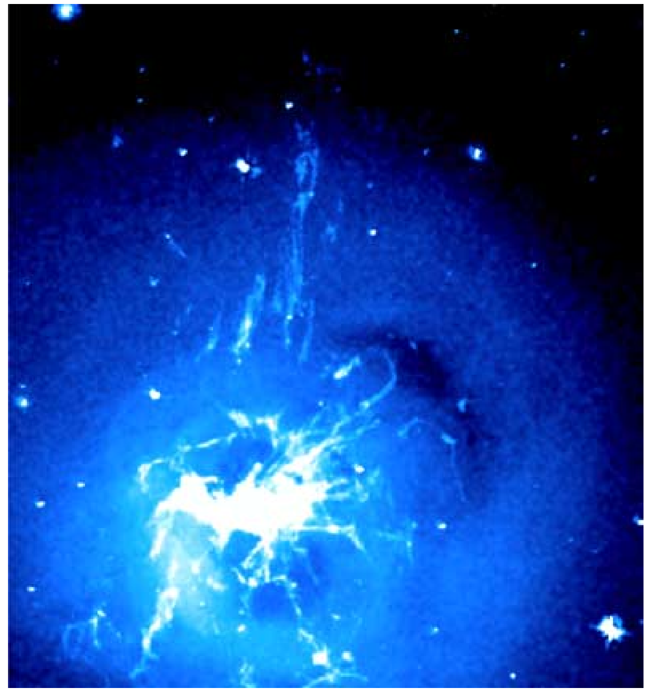

Figure 1. X-ray image of the core regions of the Perseus cluster from the *Chandra* X-ray Observatory (from Fabian et al. 2003a) overlaid with the Hα image from the Wisconsin Indiana Yale NOAO (WIYN) telescope (Fabian et al. 2003b; Conselice et al. 2001). The flattened X-ray cavity is clearly visible in the central regions of this image. Furthermore, the Hα-emitting filaments display well-defined arcs, suggestive of a vortex-like flow pattern in the region behind the buoyant cavity. This image is 4.33 arcmin (96 kpc) on a side and is oriented such that north is upwards.

With this background and motivation, this paper presents hydrodynamic simulations of the buoyant evolution of an AGN-blown cavity in a viscous ICM. In order to bring clarity to the discussion of such a complex system, this paper deals with the focused question of how ICM viscosity affects the observed morphology and associated flow patterns of old (ghost) cavities. Detailed investigations of the effects of viscosity on the growth of active cavities and the thermodynamic state of the ICM will be addressed in future work. Section 2 reviews the importance of viscosity in typical clusters, and touches upon the robustness of viscosity in the presence of magnetic fields. Section 3 describes the basic set-up of our simulations, as well as our results on the morphology and flow patterns. Section 4 discusses some of the limitations of this work, and possible implications of ICM viscosity. Finally, conclusions are presented in Section 5.

2 THE IMPORTANCE OF VISCOSITY IN THE ICM

Before discussing simulations of viscous systems, we shall address in brief the general issue of viscosity in the ICM. Initially suppose that the ICM can be described as a thermal fully ionized plasma which is unmagnetized. The relevant coefficient of viscosity is given by Braginskii (1958) and Spitzer (1962) as

$$\mu_{\rm um} = 2.2 \times 10^{-15} \frac{T^{5/2}}{\ln \Lambda}\, {\rm g\,cm^{-1}\,s^{-1}}, \quad (1)$$

where T is the temperature of the plasma measured in kelvin and $\ln \Lambda$ is a Coulomb integral. Scaling to a temperature of $kT = 5T_5$ keV and using $\ln \Lambda = 30$ gives $\mu = 1.88 \times 10^3\, T_5$ g cm^{-1} s^{-1}.

It is customary to measure the importance of viscosity in a fluid of density ρ through the Reynolds number, $\mathrm{Re} = UL/\nu$, where U and L are characteristic velocities and length-scales of the system and $\nu = \mu/\rho$. Of course, in a complicated system such as a radio-galaxy/ICM interaction, there is no unique velocity and length-scale and so it is not possible to define a universal Reynolds numbers that characterizes the system. However, provided one uses some consistent choice for U and L, the Reynolds number is still useful as a means to parametrize the relative importance of viscosity between different AGN/ICM systems. It also allows a means of matching the viscosity imposed in simulations with that expected in real systems.

We choose the maximum dimension of the bubble as our characteristic length-scale, and half of the adiabatic sound speed (i.e. a typical buoyancy-induced rise velocity) as our characteristic velocity. Scaled to the north-west ghost cavity of the Perseus cluster (with number density $n \approx 0.03$ cm^{-3}, and $kT \approx 5$ keV which gives $c_{\rm s}^2 = 780$ km s^{-1}), this gives a Reynolds number of

$$\mathrm{Re} = 62 \left(\frac{U}{390\ {\rm km\ s^{-1}}}\right)\left(\frac{L}{20\ {\rm kpc}}\right)\left(\frac{kT}{5\ {\rm keV}}\right)^{-2.5} \times \left(\frac{n}{0.03\ {\rm cm^{-3}}}\right)\left(\frac{\mu}{\mu_{\rm um}}\right)^{-1}. \quad (2)$$

We note that this Reynolds number is almost an order of magnitude smaller than the fiducial value of Re = 400 quoted by Robinson et al. (2004), primarily due to our higher (and more realistic) fiducial temperature. Thus, restating the conclusion of Fabian et al. (2003a), viscosity may be relevant to the evolution of an AGN-induced bubble in the ICM.

The major uncertainty is the effect that magnetic fields have on the macroscopic viscosity. The case of a uniform field is readily analysed (Spitzer 1962). The proton gyroradius corresponding to any non-negligible magnetic field is very small, leading to extremely efficient suppression of the local coefficient of viscosity perpendicular to the magnetic field; for typical ICM conditions, the perpendicular coefficient of viscosity is suppressed by the enormous factor of $\sim 10^{23}$ (Spitzer 1962). However, the effective macroscopic viscosity in the case of a realistic magnetic field configuration (which is almost certainly tangled, and may be chaotic) is an open question. A similar issue has recently been addressed in the context of thermal conduction. In that case, the local thermal conductivity is also suppressed by a very large factor perpendicular to the field. However, the exponential divergence of neighbouring field lines in a chaotic field structure results in an effective thermal conductivity, κ, that is suppressed below the unmagnetized value, $\kappa_{\rm um}$, by only a factor of 10^{-2}–0.2 (depending on the spectrum of fluctuations in the field structure; Narayan & Medvedev 2001). While the tensorial nature of the viscous stress tensor prevents a precise mapping of the two problems, similar arguments may apply and we might expect the effective coefficient of viscosity to be suppressed below the unmagnetized value by some factor ranging from 10^{-2} to unity.

Clearly, the effective thermal conductivity and viscosity characterizing the ICM is still very much an open theoretical question, due to uncertainties in both the basic physics of transport processes in hot plasmas as well as the magnetic field structure present in the ICM. To make progress we must *assume* that certain conditions exist, compute the consequences for radio-galaxy/ICM interactions, and compare with the recent observations. This is the motivation for the rest of this paper. While the evidence for non-negligible ICM viscosity is still circumstantial, we show that the action of such a viscosity allows the morphology of ghost cavities (in particular, the north-west ghost cavity in Perseus-A) to be reproduced, and may be an important mechanism for stabilizing the ICM core against radiative losses.

3 VISCOUS HYDRODYNAMIC SIMULATIONS

3.1 Basic set-up of the simulations

Our goal is to study the evolution of a buoyant radio lobe in the ICM of a galaxy cluster, including the effects of kinematic viscosity. Following the approach of Brüggen & Kaiser (2001), we simulate only the phase of the evolution after the radio-loud AGN has inflated a low-density bubble which has expanded to achieve pressure equilibrium with the ICM. At some point during this process, the AGN activity is assumed to cease. Thus, our simulation follows the evolution of a low-density bubble, initially in pressure equilibrium, placed in the central regions of an ICM atmosphere.

Even though real radio lobes will have rapid and complex internal flows (induced by the AGN jet during their inflation), we shall assume that both the ICM and the bubble interior are initially static. We stress that this is an important simplification in our models and must be kept in mind when interpreting the results. For example, our calculations will not be meaningful for addressing the issue of shocks and sound waves driven into the ICM by the radio galaxy, since these phenomena are almost certainly dominated by the jet-driven inflation phase of the bubble which we are not modelling. Furthermore, the precise growth rates of the RT and Kelvin–Helmholtz (KH) instabilities will be influenced by the internal motions within the bubble left over from its inflation phase. However, our set-up allows a qualitative investigation of the hydrodynamics of buoyantly rising ICM bubbles.

Our detailed set-up is as follows. The undisturbed ICM atmosphere is given a density profile described by $\rho(r) = \rho_0[1 + (r/r_0)^2]^{-0.75}$, where we choose units of mass and length such that $\rho_0 = 1$ and $r_0 = 1$. This atmosphere is assumed to be initially static and isothermal, with an adiabatic sound speed of $c_{\rm s} = 1$. The gravitational potential, Φ, is assumed to be dominated by dark matter and, hence, is assumed to be fixed throughout the simulation. This gravitational potential is determined by the condition that the initial ICM atmosphere is in hydrostatic equilibrium, $\nabla p = -\rho\nabla\Phi$, where p is the pressure. In this ICM atmosphere, we carve out a spherical bubble with density $\rho_{\rm bub} = 0.01$ and radius $r_{\rm bub} = 1/4$. This bubble is displaced from the centre of the ICM atmosphere by $\Delta r = 1/4$ (i.e. the boundary of the bubble touches the centre of the ICM atmosphere). The initial pressure of the bubble is set equal to the initial ICM pressure at that radius (i.e. this is a hot, low-density bubble in local pressure equilibrium with the ICM). We note that this is a very simplified form for the cluster density profile and gravitational potential. However, we feel that a more sophisticated cluster profile (e.g. using a Navarro, Frenk & White 1997 profile, and including the potential of the cD galaxy) would be unwarranted for the qualitative nature of the current investigation.

This initial state is evolved using the equations of three-dimensional viscous hydrodynamics,

$$\frac{D\rho}{Dt} + \rho\nabla\cdot\boldsymbol{v} = 0 \tag{3}$$

$$\rho\frac{D\boldsymbol{v}}{Dt} = -\nabla p - \rho\nabla\Phi - \nabla\cdot\boldsymbol{\Pi} \tag{4}$$

$$\rho\frac{D}{Dt}\left(\frac{\epsilon}{\rho}\right) = -p\nabla\cdot\boldsymbol{v} - \boldsymbol{\Pi} : \nabla\boldsymbol{v} \tag{5}$$

where $\boldsymbol{v}$ is the velocity field, ϵ is the internal energy density, and $\boldsymbol{\Pi}$ is the viscous stress tensor,

$$\Pi_{ik} = \mu\left(\frac{\partial v_i}{\partial x_k} + \frac{\partial v_k}{\partial x_i} - \frac{2}{3}\delta_{ik}\frac{\partial v_j}{\partial x_j}\right). \tag{6}$$

Note that we only include 'p dV' and viscous dissipation terms in the energy equation, equation (4). In particular, we neglect the radiative cooling which is unlikely to be relevant for the dynamical time-scale processes modelled here. These equations are solved using the ZEUS-MP MHD code (Stone & Norman 1992a,b), operating in Cartesian coordinates (x, y, z). ZEUS is a fixed-grid, time-explicit Eulerian code which uses an artificial viscosity to handle shocks. When operated using van Leer advection, as in this work, it is formally of second-order spatial accuracy. We model one half of the ICM atmosphere using a simulation volume of a cubic box of length $2r_0$ on a side. The cluster centre $(r = 0)$ is placed in the centre of one face of this cube, and reflecting boundary conditions are imposed on this face in order to account for the unmodelled half of the atmosphere. Outflow boundary conditions are imposed on all other faces.

The effects of viscosity are introduced into the basic ZEUS-MP code by adding explicit source terms to the momentum and energy equations (equations 4 and 5, respectively). To ensure numerical stability, the time-step on which the equations were evolved was constrained to be

$$\mathrm{d}t = \left(\mathrm{d}t_{\mathrm{visc}}^{-2} + \mathrm{d}t_{\mathrm{cour}}^{-2}\right)^{-1/2}, \tag{7}$$

where $\mathrm{d}t_{\mathrm{cour}}$ is the usual Courant–Friedrichs–Levy time-step and

$$\mathrm{d}t_{\mathrm{visc}} = \mathcal{C}_{\mathrm{visc}} \min\left[\frac{\mathrm{d}x_i^2}{\mu}\right] \tag{8}$$

is the relevant viscous time-step. In this last expression, $\mathrm{d}x_i$ is the size of a grid cell in the i-th direction, and the minimization occurs over all grid cells. On the basis of a standard stability analysis, we choose $\mathcal{C}_{\mathrm{visc}} = 0.1$.

In real systems, the interior of the ICM cavities is filled with extremely tenuous and strongly magnetized relativistic plasma; the coefficient of viscosity of this material is likely to be negligible. However, our (one-fluid) simulations model these structures simply as bubbles of very hot gas (with initial conditions of $T_{\mathrm{bubble}} = 100T_{\mathrm{ambient}}$). If we were to include the temperature dependence of μ in our calculations (equation 1), the coefficient of viscosity inside the bubble would be three orders of magnitude greater than in the ambient ICM. This is unphysical. We address this problem by fixing μ to be constant in both space and time throughout a given simulation. This choice suppresses the viscosity of the simulated hot gas inside the bubble. We note that this method avoids the need to truncate the viscosity artificially within the bubble (e.g. see Ruszkowski, Brüggen & Begelman 2004), leading to greater robustness and numerical stability. We have, however, performed additional simulations in which we do truncate the viscosity within the bubble (using a density threshold) in order to assess the impact of this assumption. Comparing those simulations with the ones presented in this paper, we confirmed that the dynamics of the buoyant bubble considered here are not qualitatively affected by the constant μ assumption.

Table 1. Basic information for the set of simulations presented in this paper.

Run	$\mu/10^{-3}$	Re	Simulation grid
1	0	$\sim 2\times 10^3$	200^3
2	1	500	200^3
3	2	250	200^3
4	4	125	200^3
5	10	50	200^3
6	20	25	200^3

Using the same definition as Section 2, the Reynolds number characterizing the hydrodynamics of the simulated bubble is

$$\mathrm{Re} \equiv \frac{vL\rho}{\mu} = 50\left(\frac{v}{2c_{\mathrm{s}}}\right)\left(\frac{L}{1\ \mathrm{unit}}\right)\left(\frac{\rho}{1\ \mathrm{unit}}\right)\left(\frac{\mu}{10^{-2}}\right)^{-1}, \tag{9}$$

where v and L are the characteristic velocity and size, respectively, of the bubble. We perform a set of simulations to explore a range of Reynolds numbers; see Table 1 for details of the runs performed.

3.2 The inviscid (control) case

Initially we discuss the results from our zero-viscosity $(\mu = 0)$ simulations. These will serve as a crucial comparison for understanding the viscous simulations that we shall discuss next. Our qualitative simulation set-up and results are very similar to those previously obtained by Brüggen & Kaiser (2001, 2002), Churazov et al. (2001), Brüggen et al. (2002) and Robinson et al. (2003). Of course, it is important to realize that even in this $\mu = 0$ cases, the action of numerical diffusion keeps the effective Reynolds number finite. We determine the effective Reynolds number of these 'zero-viscosity' cases by performing additional simulations with small values of μ and visually comparing the smallest scale structures resulting from the $\mu = 0$ run. This exercise suggests that the effective Reynolds numbers of our $\mu = 0$ simulations are in the range 2000–5000.

The initially static bubble starts accelerating due to buoyancy. As noted by several previous authors, RT instabilities induce circulatory motions within the bubbles, which then induce 'secondary' KH instabilities along the contact discontinuity between the low-density bubble and ambient ICM. These KH instabilities are primarily responsible for shredding the bubble within 2–3 time units (i.e. ∼5 sound crossing times of the bubble; top panels of Fig. 2). Due to the shredding of the bubble, one never observes a detached and flattened but otherwise intact structure such as we appear to see in the ghost cavity of Perseus-A (see bottom panels of Fig. 2).

To further facilitate comparison with observations, we produce simulated X-ray surface brightness maps. In detail, we set the local X-ray emissivity to be proportional to $\rho^2 T^{1/2}$ and integrate along lines of sight through the simulation volume in order to build up a two-dimensional map of X-ray surface brightness. For definiteness, we show surface brightness maps for the case in which the observer is viewing along the y-direction (i.e. the line joining the centre of the ICM atmosphere and the centre of the initial bubble is perpendicular to the observer's line of sight). From these maps, it can be seen that

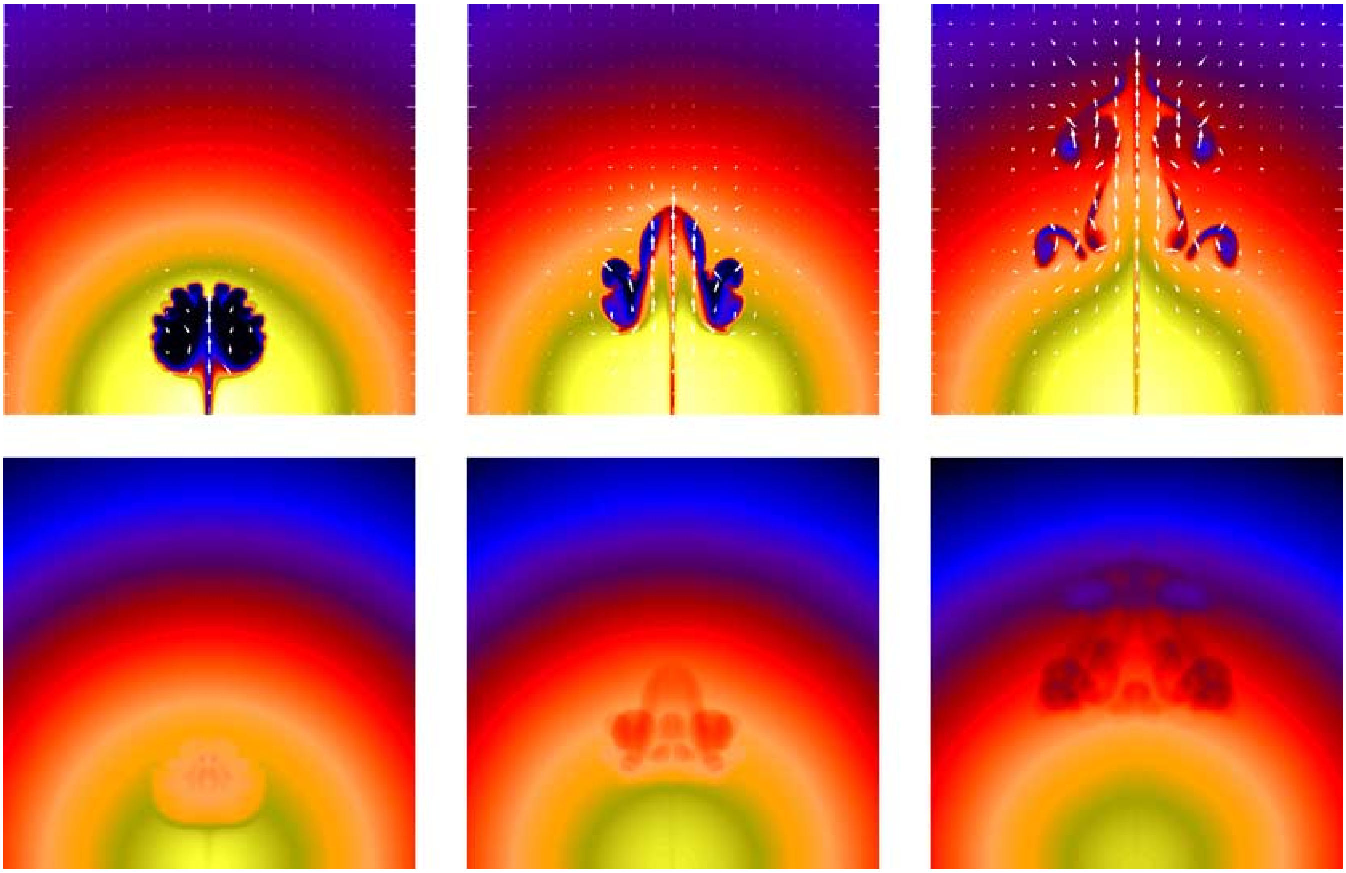

Figure 2. Mid-plane density slices (upper panels) and simulated X-ray surface brightness maps (lower-panels) for the inviscid control case (Run 1) shown at three times: $t = 1$ (left panels), $t = 2$ (middle panels) and $t = 4$ (right panels). Arrows indicating fluid velocity have been superposed on the density slices. Note how the bubble is rapidly destroyed by the combined action of RT and KH instabilities. At no time would one observe a flattened detached ghost cavity as we see in Perseus-A.

the observed cavity never has the appearance of the Perseus-A ghost cavity (Fig. 2; lower panels).

In addition to morphological problems, we note that zero-viscosity models do not reproduce the Hα-deduced flow pattern. At early times, while the buoyant bubble is still reasonably intact, we never see a circulatory flow pattern below the bubble. At late times, the buoyant bubble loses integrity and induces complex and disorganized motions in the ICM.

3.3 Simulations including viscosity

Having described the inviscid 'control' case, we now proceed to discuss the effect of viscosity on the buoyant evolution of radio lobes. As in the inviscid case, the evolution is driven by the joint action of buoyancy and secondary KH instabilities. However, unlike the inviscid case where KH instabilities operate at the contact discontinuity on spatial scales down to the grid scale, viscosity suppresses the KH instability on small spatial scales. This has a profound effect on the evolution of the bubble; even a moderate amount of viscosity can prevent the shredding of the bubble, which can subsequently float out of the core, being rather flattened but otherwise intact.

As a specific example, Fig. 3 shows the Re = 250 (Run 3). This can be considered a model of the ghost cavities around Perseus-A if the ICM possesses a coefficient of viscosity of $\mu \approx 0.25\,\mu_{\rm um}$. As discussed in Section 2, this level of viscosity may be plausible even in the presence of tangled, chaotic magnetic fields. It can be seen from the mid-plane density and velocity fields (Fig. 3; upper panels) that the evolution of the bubble is driven by buoyancy, with secondary KH instabilities largely unable to overcome the action of the viscosity. As the bubble floats upwards, it flattens into a broad cap. The surface brightness maps associated with Run 3 (Fig. 3; lower panels) show that one does, indeed, produce a detached and flattened cavity in the ICM emission as observed in the Perseus cluster.

Fig. 4 shows results for the full range of viscosity explored in this paper at three fixed times ($t = 1, 4, 8$). It can be seen that the formation of a flattened but intact buoyant bubble occurs in all of our viscous simulations. However, the time-scale on which the evolution proceeds is a strong function of the viscosity. For example, the $t = 1$ density slice of Run 2 (Re = 500) is very similar to the $t = 4$ slice of Run 6 (Re = 50). This fact may point to a solution of the 'shock problem' noted in the introduction, an issue that we shall return to in Section 4.2.

Viscosity also has important implications for the flow pattern in the disturbed ICM. In principle, the presence of viscosity can facilitate the development of large-scale vortex rings in the trailing region beneath the rising bubble. This phenomenon is seen for our highest viscosity cases. For the levels of viscosity that are probably relevant to the Perseus cluster (Re = 100–200), this effect is not seen. However, even for these levels of viscosity, our simulations show flow patterns that qualitatively match those inferred from the Hα-filament geometry in Perseus. In these cases, the flattened buoyant bubble

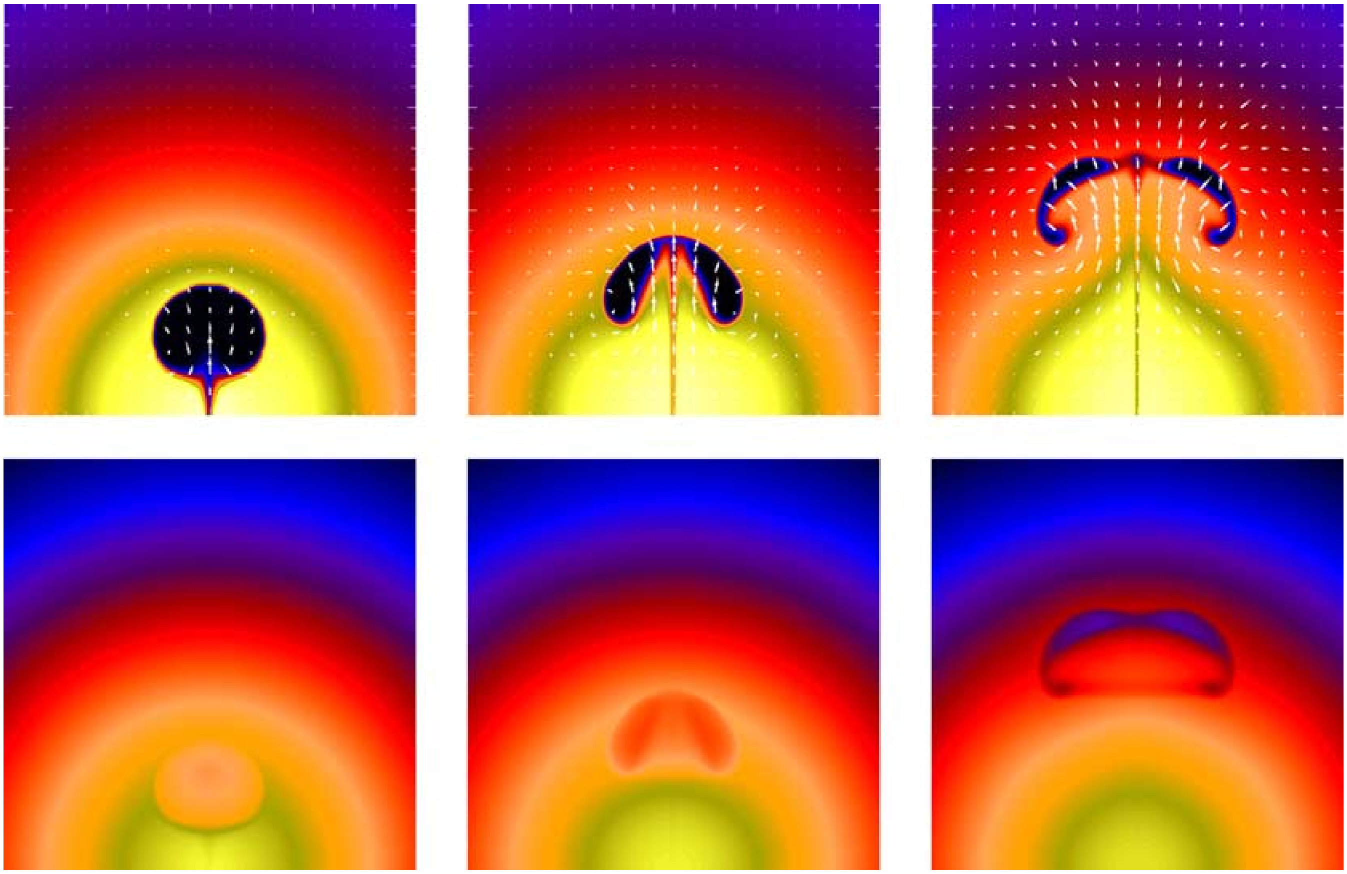

Figure 3. Mid-plane density slices (upper panels) and simulated X-ray surface brightness maps (lower-panels) for the Re = 250 case (Run 3) shown at three times: $t = 1$ (left panels), $t = 2$ (middle panels) and $t = 4$ (right panels). Arrows indicating fluid velocity have been superposed on the density slices. Note how the viscosity stabilizes the bubble, allowing a flattened but intact buoyant 'cap' to form. Both the X-ray surface brightness and Hα-inferred velocity field around the ghost cavity of Perseus-A can be qualitatively reproduced by this model.

undergoes a minor fragmentation due to the action of secondary KH instabilities. As a result of this fragmentation, a small torus of radio plasma is left in the trailing region behind the main buoyant bubble. The simulations show a strong ICM circulation around this trailing torus, producing streamlines that resemble the Hα-filament geometry in Perseus. A prediction of this model is that sufficiently sensitive X-ray maps should reveal subtle depressions at the centre of these vortices, and sufficiently sensitive and spatially resolved low-frequency radio maps should reveal a corresponding torus of aged radio plasma.

An important consequence of ICM viscosity is that it provides an explicit mechanism by which the radio-galaxy induced disturbance can heat the ICM. While a full treatment of viscous ICM heating by radio galaxies almost certainly requires following the jet-driven inflation of the bubbles (e.g. Reynolds, Heinz & Begelman 2002), as well as multiple epochs of activity (Ruszkowski et al. 2004), it is instructive to compute the viscous dissipation rate in our idealized simulation. Fig. 5 shows the dissipation rate as a function of time for our canonical 'Perseus-like' model, the Re = 250 case. The dissipation rate and the time coordinate are given in physical units assuming parameters relevant to the Perseus cluster (see caption of Fig. 5). The dissipation rate displays two peaks. The rather broad peak centred at about 90 Myr coincides with the secondary KH instability entering the strongly non-linear regime, and the subsequent 'folding' of the flattened bubble. The second and rather sharp peak corresponds to the venting of material out of the boundary of the simulation and, hence, should not be considered physical. In general, the dissipated power achieves the rather modest levels of $P \sim 10^{41}$ erg s^{-1}. However, this heat source continues to operate for a period of about 200 Myr, an order of magnitude more than the plausible recurrence time-scale of the radio-galaxy activity (Fabian et al. 2003a). Thus, the possibility of balancing the radiative losses with viscous dissipation from the combined effect of many bubbles remains open. Furthermore, it is likely that the dissipation of the fluid modes driven by the initial inflation of the bubble (and hence not modelled here) will deliver just as much energy as, if not more than, the viscous dissipation during the buoyant phase.

4 DISCUSSION

4.1 The neglect of a jet and magnetic fields

Our simulations must be viewed as a rather limited toy model for the buoyant evolution of radio lobes and the formation of ghost cavities. We have employed two major simplifications. First, we have not modelled the jet-driven inflation of the bubble. Real examples of these radio lobes will possess complex, jet-driven flows with speeds much in excess of the ICM sound speed, and will never resemble the static bubbles that we use for our initial conditions (Reynolds et al. 2002). Consequently, the KH instability will be important at all stages in the life of the bubble, and does not need to wait for the RT instability to first induce bulk flows.

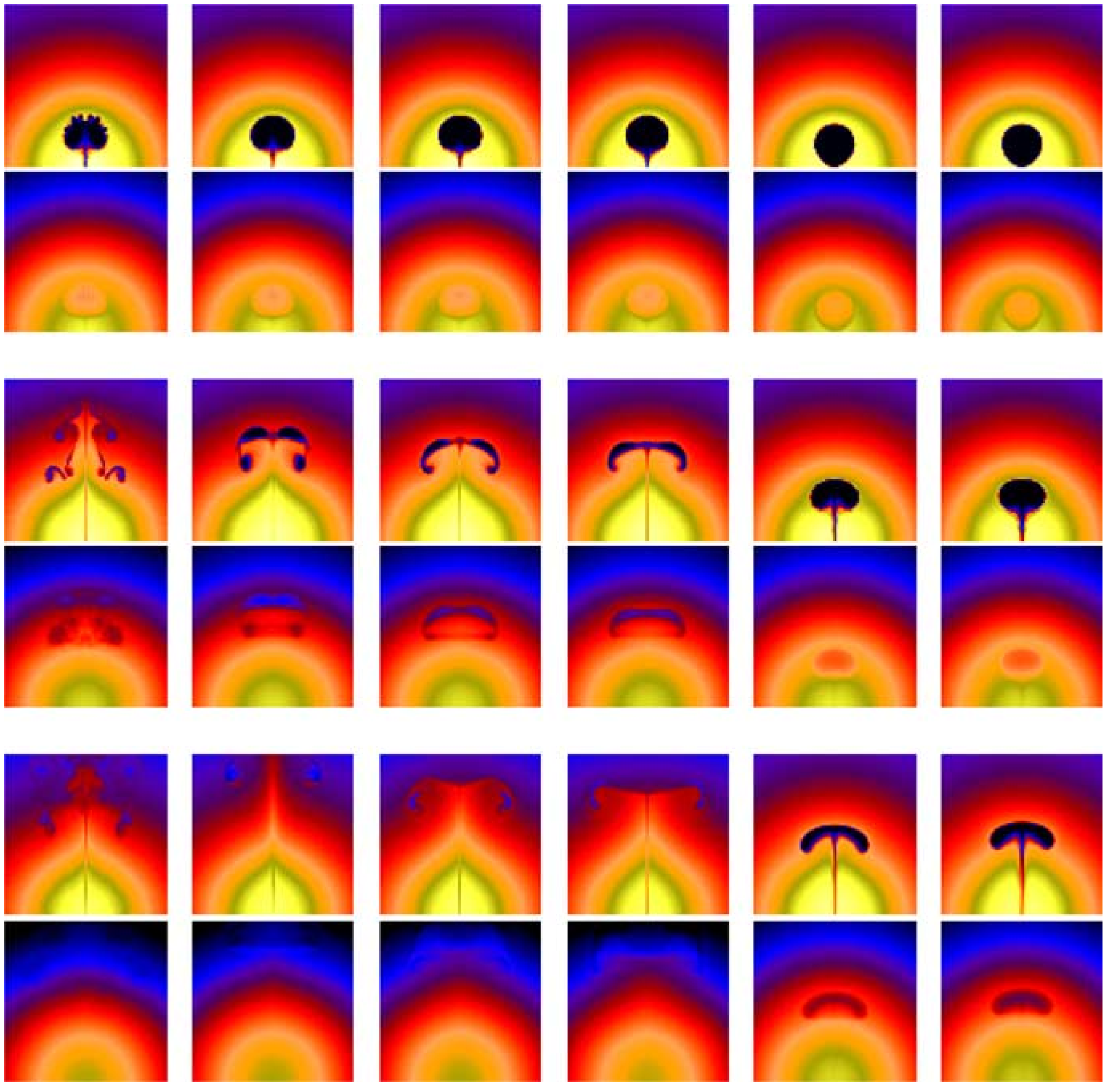

Figure 4. Mid-plane density slices (upper panels of each set) and simulated X-ray surface brightness maps (lower panels of each set) for the six simulations presented in this paper (Runs 1–6 ordered from left to right). Results are shown for three times: $t = 1$ (upper set of panels), $t = 4$ (middle set of panels) and $t = 8$ (lower set of panels). See text for a discussion of these results.

Secondly, we have neglected the effects of magnetic fields. It is expected that fields within the radio plasma could readily achieve equipartition strengths and hence have an important effect on the dynamics of the rising bubble. In particular, magnetic fields will influence the development of both the RT and the KH instability at the contact discontinuity. The effect of magnetic fields on the buoyant evolution of ICM bubbles has recently been addressed in the context of inviscid hydrodynamics by Brüggen & Kaiser (2001), De Young (2003) and Robinson et al. (2003). Their results suggest that magnetic fields can have a strongly stabilizing effect on buoyant bubbles, effectively quenching all of the instabilities that distort and eventually shred this structures. However, both the symmetry of their calculation (two-dimensional Cartesian) and their initial magnetic field configuration (taken from Cargill et al. 1996) make the Robinson et al. (2003) calculation most relevant to a buoyantly rising *cylindrical flux tube with purely toroidal magnetic flux*, a poor approximation to an AGN-blown bubble. The ability of magnetic fields to stabilize or destabilize the contact discontinuity is a strong function of the magnetic configuration and field strength (e.g. see Jun, Norman & Stone 1995), both of which are open issues in the case of AGN-blown bubbles.

Clearly further simulations are required to address these two issues. In fact, it would be most appropriate to treat these as coupled questions. It is believed that the magnetic field in such bubbles originates from the magnetized AGN jets. Thus, we must follow the jet-driven inflation of the bubble in order to produce a reasonable initial field configuration. This will be the subject a future publication.

4.2 Can viscosity solve the 'shock problem'?

In addition to stabilizing buoyant radio lobes against shredding, we have discussed how viscosity can dramatically slow the evolution of the bubble. This suggests a natural solution to the 'shock problem' noted in the introduction. Under the action of viscosity, the AGN jets may inflate their ICM bubbles subsonically before the buoyancy effects become important. Consequently, the ICM can be displaced into a cavity-bounding shell without the need of a strong shock. The thermal structure of this gas will be determined by the action of compression (due to its displacement from the cavity), decompression (due to the fact that this material will typically be lifted to a higher level in the ICM atmosphere), viscous

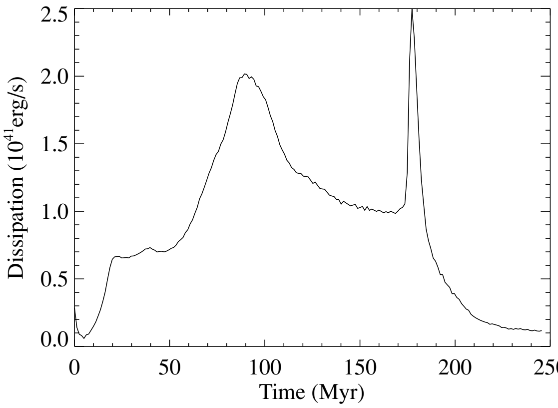

Figure 5. Volume integrated viscous dissipation rate for our Re = 250 case, scaled with parameters relevant for the Perseus cluster (i.e. the simulation domain has a linear size of 40 kpc in each dimension, one code unit of density is 0.03 cm^{-3}, and the initial ICM sound speed is 780 km s^{-1}). One code unit of time is then 24 Myr. As noted in the main text, the second and rather sharp peak in the dissipation rate is likely due to an interaction of the flow pattern with the boundaries of the computation and hence should not be considered physical.

dissipation, and radiative cooling. One can envisage a scenario in which the rather slow evolution of the radio lobe in a viscous ICM allows the shell of displaced ICM to cool radiatively by an appreciable amount. Further simulations of the inflation stage of these bubbles are required to assess whether the rather cool cavity-bounding shells observed in Perseus-A can be reproduced within the context of this model. Given the strong temperature dependence of the coefficient of viscosity (equation 1), we might expect significant changes in the effective viscosity between the various ICM structures defining the system (i.e. the ambient material, the cool rims and the shocks, if any). Thus, it will be important to move beyond the constant μ assumption in the next generation of simulations.

5 CONCLUSIONS

The true role of kinematic viscosity in ICM/radio-galaxy interactions remains unclear, primarily due to the great uncertainty associated with magnetic suppression of Spitzer-type transport processes in the plasma. However, in stark contrast to the inviscid models, our models of bubble evolution in modestly viscous ICMs can reproduce both the morphology and inferred flow patterns seen around the best-studied of the ghost ICM cavities, the north-west cavity in Perseus-A. The principal effect of viscosity is to stabilize the bubble against both RT and KH instabilities, thereby allowing it to remain intact as it floats upwards in the ICM atmosphere. The flattening of such bubbles as they rise is a natural explanation for the elongated morphology of the north-west cavity in Perseus-A. The 'smoke-ring' like flow pattern below the north-west cavity inferred from the morphology of the Hα filaments can then arise due to minor fragmentation of the rising bubble (leading to a trailing torus) or genuine vortex shedding.

If the ICM is indeed viscous at the level treated by our models, the subsequent slowing of the evolution time-scales for ICM/radio-galaxy interactions may be the solution to the 'shock problem', i.e. the lack of strong shocks bounding the ICM cavities that are associated with active radio lobes. In this scenario, radio galaxies such as Perseus-A would be rather less powerful than previously thought (Heinz et al. 1998), inflating their associated ICM bubbles subsonically. If the evolution is sufficiently slow, radiative cooling might allow the ICM shell surrounding the cavity to cool, again in agreement with *Chandra* observations of Perseus-A.

Ultimately, disentangling the effects of transport processes (viscosity and thermal conduction) and magnetic fields will require further simulation work coupled with detailed observations. On the theoretical side, it is important to initiate a new generation of simulations which incorporate full MHD *as well as* transport processes. Qualitatively new and rich dynamics become possible upon the inclusion of transport processes within MHD. For example, Balbus (2000) discovered the 'magnetothermal instability' which occurs in any MHD atmosphere with a temperature profile that decreases with height provided there is thermal conduction along the magnetic field lines. In addition, the viscous transport coefficients will be anisotropic in the presence of a magnetic field, and this may lead to yet further complexity in the dynamics. Such instabilities could well be crucial for understanding the dynamics of radio-galaxy/ICM interactions. Observationally, deep (megasecond) *Chandra* observations of the nearest radio-galaxy/cluster interactions might allow detailed imaging spectroscopy of fluid instabilities associated with the radio-galaxy/ICM interaction. Furthermore, upon the launch of *Astro-E2* in 2005, we will be able to probe turbulent velocities directly within the ICM of nearby (bright) clusters through broadening of their X-ray emission lines. With the caveat that full MHD viscous simulations have yet to be done, the presence or absence of turbulence in the ICM, especially in regions well separated from potential driving sources (such as AGN or merging subclusters), could be an important indicator of the presence of viscosity.

ACKNOWLEDGMENTS

We thank Cole Miller and Eve Ostriker for stimulating conversations conducted throughout the course of this work. We gratefully acknowledge support from the National Science Foundation under grant AST0205990 (CSR), the *Chandra* Cycle-5 Theory & Modelling program under grant TM4-5007X, and the Royal Society (ACF). All simulations presented in this paper were performed on the Beowulf cluster in the Department of Astronomy at the University of Maryland, kindly administered by Derek Richardson.

REFERENCES

Balbus S. A., 2000, ApJ, 534, 420
Blanton E. L., Sarazin C. L., McNamara B. R., Wise M. W., 2001, ApJ, 558, L15
Böhringer H., Voges W., Fabian A. C., Edge A. C., Neumann D. M., 1993, MNRAS, 264, L25
Böhringer H., Nulsen P. E. J., Braun R., Fabian A. C., 1995, MNRAS, 274, L67
Braginskii S. L., 1958, Sov. Phys. JETP, 6, 358
Brüggen M., Kaiser C. R., 2001, MNRAS, 325, 676
Brüggen M., Kaiser C. R., 2002, Nat, 418, 301
Brüggen M., Kaiser C. R., Churazov E., Enssline T. A., 2002, MNRAS, 331, 545
Cargill P. J., Chen J., Spicer D. S., Zalesak S. T., 1996, J. Geophys. Res., 101, 4855
Carilli C. L., Perley R. A., Harris D. E., 1994, MNRAS, 270, 173
Choi Y. Y., Reynolds C. S., Heinz S., Rosenberg J. L., Perlman E. S., Yang J., 2004, ApJ, 606, 185
Churazov E., Brüggen M., Kaiser C. R., Böhinger H., Forman W., 2001, ApJ, 554, 261
Clarke D. A., Harris D. E., Carilli C. L., 1997, MNRAS, 284, 981

Conselice C. J., Gallagher J. S., Wyse R. F. G., 2001, AJ, 122, 2281
David L. R. et al., 2001, ApJ, 557, 546
De Young D. S., 2003, MNRAS, 343, 719
Fabian A. C. et al., 2000, MNRAS, 318, L65
Fabian A. C., Celotti A., Blundell K. M., Kassim N. E., Perley R. A., 2002a, MNRAS, 331, 369
Fabian A. C., Voigt L. M., Morris R. G., 2002b, MNRAS, 335, L71
Fabian A. C. et al., 2003a, MNRAS, 344, L43
Fabian A. C., Sanders J. S., Crawford C. S., Conselice C. J., Gallagher J. S., Wyse R. F. G., 2003b, MNRAS, 344, L48
Feigelson E., Wood P. A. D., Schreier E. J., Harris D. E., Reid M. J., 1987, ApJ, 312, 101
Harris D. E., Carilli C. L., Perley R. A., 1994, Nat, 367, 713
Heinz S., Reynolds C. S., Begelman M. C., 1998, ApJ, 501, 126
Heinz S., Choi Y. Y., Reynolds C. S., Begelman M. C., 2002, ApJ, 569, L79
Jun B., Norman M. L., Stone J. M., 1995, ApJ, 453, 332
Kim W. T., Narayan R., 2003, ApJ, 596, 889
Matsushita K., Belsole E., Finoguenov A., Böhringer H., 2002, A&A, 386, 77
McNamara B. R. et al., 2000, ApJ, 534, L135
McNamara B. R. et al., 2001, ApJ, 562, L149
Narayan R., Medvedev M. V., 2001, ApJ, 562, L129
Navarro J. F., Frenk C. S., White S. D. M., 1997, ApJ, 490, 493
Owen F. N., Eilek J. A., Kassim N. E., 2000, ApJ, 543, 611
Peterson J. A. et al., 2001, A&A, 365, 104
Reynolds C. S., Heinz S., Begelman M. C., 2002, MNRAS, 332, 271
Robinson K. et al., 2004, ApJ, 601, 621
Ruszkowski M., Brüggen M., Begelman M. C., 2004, ApJ, 611, 158
Sanders J. S., Fabian A. C., 2001, MNRAS, 331, 273
Spitzer L., 1962, The Physics of Fully Ionized Gases, 2nd edn. Interscience, New York
Stone J. M., Norman M. L., 1992a, ApJS, 80, 791
Stone J. M., Norman M. L., 1992b, ApJS, 80, 81
Tamura T. et al., 2001, A&A, 365, L87
Voigt L. M., Schmidt R. W., Fabian A. C., Allen S. W., Johnstone R. M., 2002, MNRAS, 335, L7
Young A. J., Wilson A. S., Mundell C. G., 2002, ApJ, 579, 560

This paper has been typeset from a TEX/LATEX file prepared by the author.